A novel porous Ti6Al4V: Characterization and cell attachment

J. P. Li,[1,3] S. H. Li,[2] C. A. Van Blitterswijk,[1] K. de Groot[1,2]
[1]*iBME, Twente University, Prof Bronkhorstlaan 10-D, 3723 MB Bilthoven, The Netherlands*
[2]*CAM Implants, Zernikedreef 6, 2333CL, Leiden, The Netherlands*
[3]*Beihang University, School of Mechanical Engineering & Automation, 100083, Beijing, China*

Received 5 January 2004; revised 9 November 2004; accepted 17 November 2004
Published online 10 March 2005 in Wiley InterScience (www.interscience.wiley.com). DOI: 10.1002/jbm.a.30278

Abstract: For the first time, a highly porous strong Ti6Al4V was produced by using a "polymeric sponge replication" method. A polymeric sponge, impregnated with a Ti6Al4V slurry prepared from Ti6Al4V powders and binders, was subjected to drying and pyrolyzing to remove the polymeric sponge and binders. After sintering at a high temperature and under high vacuum, a porous Ti6Al4V was produced. Optical microscopical observation, environmental scanning electron microscopy observation (with energy-dispersive micro X-ray analysis), mechanical tests, and metallurgical analyses were performed on the obtained porous Ti6Al4V with regard to the porous structure (both macropores and micropores), mechanical properties, chemical composition, phase compositions, and cell attachment behavior. The porous Ti6Al4V made by this method had a three-dimensional trabecular porous structure with interconnected pores mainly ranging from 400 to 700 μm and a total porosity of about 90%. The compressive strength was 10.3 ± 3.3 MPa and the elastic constant 0.8 ± 0.3 GPa. MC3T3-E1 cells attached and spread well in the inner surface of pores. Being similar to cancellous bone with regard to both interconnected porous structure and mechanical properties, the resulting porous Ti6Al4V is expected to be a promising biomaterial for biomedical applications. © 2005 Wiley Periodicals, Inc. J Biomed Mater Res 73A: 223–233, 2005

Key words: Ti6Al4V; porous; sintering; mechanical properties; cell attachment

INTRODUCTION

Titanium and its alloys have been widely used in orthopedic and dental devices because of their excellent properties: 1) good biocompatibility; 2) high ratio of strength to weight; 3) relative low elastic constant; 4) superior corrosion resistance as compared with other metallic biomaterials, such as cobalt alloy and stainless steel.[1–3] Up to present, most implants of titanium (and its alloys) are in dense forms; however, with dense forms, problems, such as interfacial instability with host tissues, biomechanical mismatch of elastic constant, and lack of biological anchorage for tissue ingrowth, may occur.[4,5] Regarding the long-term load-bearing implant, a successful performance of implants requires reliable anchoring implants into host tissue. The advantage of porous materials is their ability to provide biological anchorage for the surrounding bony tissue via the ingrowth of mineralized tissue into the pore space.[6–10] Several factors may affect ingrowth of bone into the pore spaces of these implants, such as the porous structure (pore size, pore shape, porosity, and interconnectivity) of the implant material, the duration of implantation, biocompatibility, implant stiffness, and the micromotion between the implant and adjacent bone.[11–15] It has been shown in the literature that the architecture of a porous implant has a great effect on the bone ingrowth into the pore space.[16,17] For instance, optimal pore size for bone ingrowth is between 100–500 μm, and the pores must be interconnected to maintain the vascular system required for continuing bone development. A three-dimensional open porous structure is particularly suitable for implant fixation by tissue ingrowth.[6,18]

There are two types of porous implants: either they have a porous surface or they are completely porous (porous bulk implant).

As for orthopedic and dental implants, the need for mechanical interlock of bone or other connective tissues with an implant surface that gives secure implant fixation, is the primary reason for using porous-surfaced implants. Porous surface coating was developed for orthopedic replacement devices in the early 1970s.[19–21] Generally, porous coatings are obtained by sintering uniform-sized beads or

Correspondence to: J. P. Li; e-mail: j.li@tnw.utwente.nl
Contract grant sponsor: IsoTis S.A.

TABLE I
Comparison of the Merits and Drawbacks of the Porous Titanium Made by Powder Metallurgy

Method	Material	Advantages	Drawbacks
Pressure shaping	Ti beads[22,28,29]	Practical easiness to make. Interconnected pores. Narrow pore-size distribution.	Low porosity (<45%). Pore size as function of the particle size.
	Ti mesh[20,30–32]	Interconnected pores.	Difficult to form low porosity.
	Ti powder + pore-former[33]	Easy method in principle. Porosity up to 80%. Controllable pore size and porosity.	Difficult to control pore interconnectivity and open pore.
Pressureless shaping	Ti beads[4,34]	Easiness to make. Interconnected pores. Narrow pore-size distribution.	Low porosity (<45%). Pore size as function of the particle size.
Special shaping—plasma spray	Ti powder[19]	Commercially most successful for surface coating.	Lack of interconnected pores. Small pore size. Varied porosity.

fibers by isostatic pressing sintering or loosely packing sintering[22–27] on the dense cores. The solid cast or machined core provides necessary mechanical strength and the porous surface allows for bone ingrowth.

A brief description and comparison of methods to produce porous bulk titanium and its alloys are summarized in Table I. The successful clinical applications were attributed to the advantages of these methods.[25,35] However, their remaining drawbacks led scientists to investigate better porous structures, especially where better control over interconnectivity and porosity is concerned.

To meet practical requirements of bone ingrowth and long-term implantation, there is a need to manufacture an implant that mimics the architecture of natural bone, encourages bone to grow into the pore spaces, and provides a biological interlock between the implant and surrounding bone.

The purpose of this study, therefore, was to develop a new method to produce porous Ti6Al4V with a reticulate structure that has the following features: 1) all the pores open and interconnected in any direction; 2) structure similar to that of natural cancellous bone; 3) relative high compressive strength with its high porosity; 4) good cell attachment.

MATERIALS AND METHODS

Raw materials

Ti6Al4V powders with a mean diameter of 45 μm (Bongen Titanium Co., Ltd., China) were used in this study, together with polyurethane (PU) sponge with the specification of 3.31R45 (Calligen Europe B.V., The Netherlands). Cancellous bone samples were obtained by boiling goat cancellous bone for 1 week to remove collagen and other components.

Porous Ti6Al4V from polymeric sponge replication

Preparation of Ti6Al4V slurry

The Ti6Al4V powders (75 wt %) were mixed with H_2O (18.5 wt %). Polyethylene glycol 4000 (PEG4000; Fluka Chemie GmbH, Germany) and methylcellulose (MC, Fisher Scientific B.V., The Netherlands) were used as binders (3.5 wt %). One weight percentage of Dolapix (Aschimmer & Schwarz GmbH, Germany), 1 wt % of ammonia solution (25 wt %, Merck), and 1 wt % of 1-octanol (Acros Organics, Pittsburgh, PA) were mixed to improve the rheological property of the slurry.

Shaping

Porous Ti6Al4V green bodies were made by thoroughly dipping the polymeric sponges into the Ti6Al4V slurry. This dipping process was repeated until all the struts of the PU sponge were covered with slurry. Excess slurry was removed by using a roller-pressing device. The samples were then dried for 3 h at 80°C and for at least 24 h at room temperature.

An equivalent model for measuring surface roughness was made together with the sample batch because of difficulties in measuring directly the surface roughness inside the pores of porous Ti6Al4V made by polymeric sponge replication. To that purpose, a Ti6Al4V plate, covered with Ti6Al4V slurry was sintered under the same conditions as for the real porous samples. We assumed the surface rough-

ness of this model to be an indication of that of the inner walls of the porous Ti6Al4V made via the sponge replication process.

Removal of sponge and binder

Before the samples were put into the furnace chamber, 1.0 wt % of titanium hydride of the total sample weight was placed on both the bottom and the top of the samples and in different locations in the furnace. Before debinding, the vacuum pump was used to remove air from the furnace chamber. As the first step, argon gas was flushed into the chamber and subsequently removed by the vacuum pump. This process was repeated twice to prevent potential chemical contamination from atmospherical impurities. Removal of binders and sponge was performed while pressurized argon gas flowed through the furnace under a controlled heating rate. Thermogravimetric analysis (TGA) (PerkinElmer, software of Pyris windows) of the sponge and binder was used as the base for the design of an optimized heating profile. The final heating profile was as follows:

RT 150 min → 150°C 720 min → 400°C 150 min →
500°C 120 min → 500°C 600 min → RT

Sintering

The samples after the removal of sponge and binders were eventually sintered in a high-vacuum furnace (10^{-5} mbar) with heating profile as follows:

RT 600 min → 500°C 450 min → 1250°C 120 min →
1250°C furnace cooling → 25°C

Characterization

General

Porous Ti6Al4V prepared in the present study was characterized for geometry and porosity, chemical composition, microstructure, and mechanical properties using a stereo optical microscope (Nikon SMZ-10A with Sony progressive 3CCD color video camera) and environmental scanning electron microscope (ESEM) (model XL-30; Philips, Eindhoven, The Netherlands) together with energy-dispersive micro X-ray (EDX) analysis and a mechanical testing machine (Zwick50, Germany).

Pore structure

The characterization of the porous structure included mean pore size, uniformity of porous structure, porosity, interconnectivity, and inner surface pattern of pores.

To measure the pore size, 10 samples were cut from different porous Ti6Al4V blocks using a WOCO50 sawing machine and a WOCO 997 sawing blade (Wolfgang Conrad), and then the cross-sections were polished with a series of SiC papers. After being cleaned in an ultrasonic water bath and dried, the samples were put directly into the ESEM. Under the same magnification (15×), 10 random pores in each sample were measured and imaged, and then used for calculating the mean pore size, standard deviation, and pore-size distribution indication. Micropores on the inner surface were measured similarly to determine mean pore size. A sample was put in the ESEM and, under high magnification (500×), the surface within a pore was clearly visible, allowing micropore size to be measured.

Porosity (in percentage of volume) was calculated by two methods: 1) porosity (ρ) was calculated by measuring the apparent density (ρ_b = weight of sample/volume of sample) of sample by using the formula: $\rho = (1 - \rho_b/\rho_s) \times 100$, where ρ_s is the density of 100% dense material. A total of 10 samples were measured. 2) Porosity was estimated using quantitative analysis. The cross-sectioned sample was prepared and cleaned to remove any shaving trapped in the cutting process. After cleaning, the sample was embedded in a viscous epoxy and then evacuated to ensure that the epoxy fully penetrated the open cell structure. Next, it was prepared through standard metallographical procedures, and photographed using an inverted stage reflecting light microscope. A selected region of the image was analyzed and two counts were made, one of the black pixels and one of the total pixels in the region. The ratio of the number of black pixels to the total pixels in the region represented the fractionary porosity of the porous body.

Microstructure of inner surface wall of the pores: an inner surface roughness profile was scanned using a noncontact laser profilometer (UBM Measurement System A538, The Netherlands) and surface roughness was calculated according to DIN4768. In addition, we used an equivalent model sample, consisting of a Ti6Al4V plate with a powder layer, for three reasons: 1) to compare the inside of porous Ti6Al4V with bead surface coating; 2) to conveniently look at a surface; 3) to easily measure surface roughness.

Chemical analysis

An EDX spectrum of a porous Ti6Al4V sample was made to determine the spectrum of porous Ti6Al4V. The oxygen, carbon, and nitrogen contents were analyzed for the raw Ti6Al4V powders, the debinded Ti6Al4V powders (after removal of sponge and binders), and sintered Ti6Al4V. The carbon and nitrogen contents were measured according to ASTM D5271, and the hydrogen and oxygen contents were measured according to JGKJ121.18-2001 (Chinese standard).

Mechanical properties

Fifteen porous Ti6Al4V samples with a size of ∅10 × 11 mm were prepared using a wire electrical discharge machine. The compressive strength was determined using a

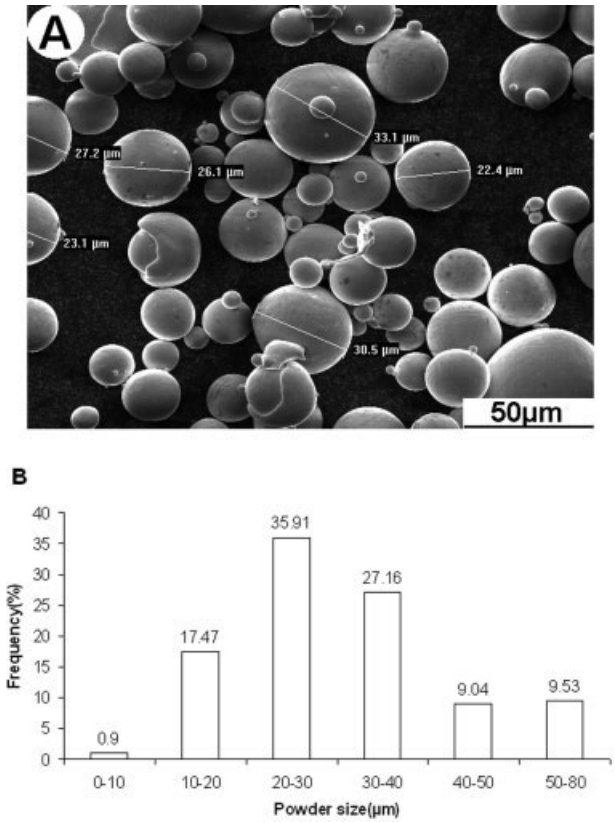

Figure 1. Ti6Al4V particle shape and size distribution of (A) particles under ESEM and (B) particle-size distribution.

mechanical testing machine at a crosshead speed of 1 mm/min.

Metallurgical analysis

Standard metallurgical techniques were applied with the porous Ti6Al4V samples to analyze the microstructure generated by heat treatment. Samples were sectioned by using a WOCO50 sawing machine. Primary polishing was accomplished by grinding with no. 320 SiC paper, followed by nos. 600, 1200, and 2000 SiC papers, respectively. Fine polishing was accomplished by using 1 micron diamond paste, followed by a 0.05-μm alumina as its final step. Etching was performed using a solution of 95% distilled water and 5% hydrofluoric acid. The etchant was applied on the sample surface by swabbing with cotton for 3–5 s. Samples were then rinsed with water, and dried by blowing air onto the surface.

Cell attachment study

MC3T3-E1 osteoblast-like cells were used for cell attachment study. The culture medium used was α-minimum essential medium supplemented with 10% fetal bovine serum (Life Technologies, The Netherlands), antibiotics, and 1% sodium pyruvate. The cells were seeded on porous Ti6Al4V samples placed in 20-well plates at 1.2×10^6 cells per sample in 4 mL of medium, and cultured at 37°C in a humidified atmosphere with 5% CO_2 and 95% air. After being cultured for 4 h and 3 days, respectively, the samples ($n = 2$) were fixed and then rinsed with phosphate-buffered saline, dehydrated in a graded ethanol series, critical point dried, sputter coated with carbon, and examined with ESEM. Other samples ($n = 3$) were digested with proteinase K (Sigma, The Netherlands), added with heparin (Leo Pharm, The Netherlands) and ribonuclease A (Sigma, The Netherlands), then shaken and incubated at 56°C for 16 h. A volume of 100 μm solution of each sample was mixed with 100 μm Cyquant GRDye (Molecular Probes, Poland), and the fluorescence using a fluorimeter (PerkinElmer) was measured at an emission wavelength of 520 nm and excitation of 480 nm. The DNA content of cells attached on the porous samples was counted through a premade standard DNA curve. DNA content was expressed as mean ± SD.

RESULTS

Raw materials characterization

Figure 1(A) illustrates an image of Ti6Al4V powder under ESEM. It shows that all powders are spherical in shape. The chemical composition of Ti6Al4V powder and the requirement of ISO5832 standard are listed in Table II. The distribution of the particle size of Ti6Al4V powder can be seen in Figure 1(B); the majority (~50%) is between 10 and 30 μm, a range that facilitated the preparation of Ti6Al4V slurry and later its sintering. The smaller the particle size, the lower the sedimentation speed; however, fine powders can be sintered more readily than coarse ones. Figure 2 shows that the pores of sponge are well interconnected.

The results from the removal of sponge and binders by TGA measurement are illustrated in Figure 3. It reveals that most of the sponge and binders pyrolyzed

TABLE II
Chemical Composition of Ti6Al4V Powder

	Element (wt %)								
	Al	V	N	H	O	C	Fe	Si	Ti
Ti6Al4V	6.47	4.08	0.025	0.008	0.183	0.02	0.12	0.04	Bal
ISO5832	5.5–6.8	3.5–4.5	0.05	0.015	0.20	0.08	0.3	0.04	Bal

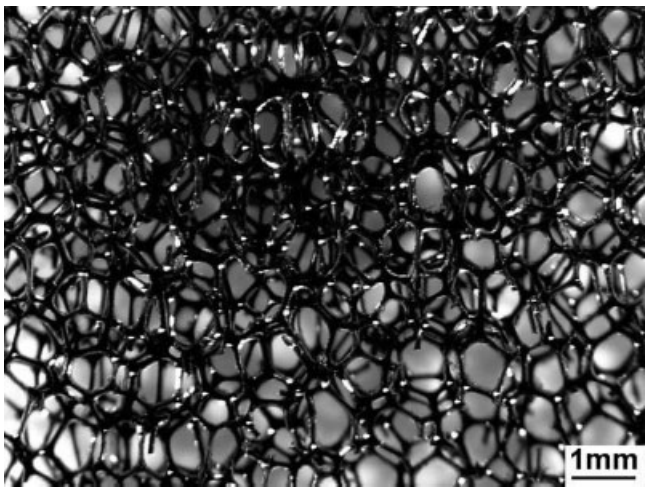

Figure 2. PU sponge under optical micrograph.

between 150° and 400°C. To complete this pyrolysis process, the debinding temperature was set at 500°C under flowing argon atmosphere.

Shrinkage of porous Ti6Al4V

The dimension of a sample was 100 × 15 × 30 mm before sintering and 91.5 × 13.7 × 25.6 mm after sintering at 1250°C for 2 h. Consequently, the horizontal linear shrinkage rate was about 8.5%, and the vertical linear shrinkage 14.7%, corresponding to a volumetric decrease of 28.7%.

Structural analysis

Macroporous structure of porous Ti6Al4V and cancellous bone

Figure 4(A,B) shows the macrostructures of our porous Ti6Al4V and goat cancellous bone using ESEM.

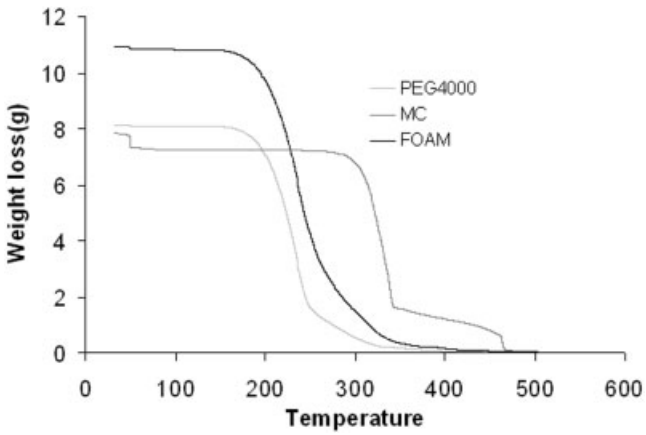

Figure 3. TGA curves of PEG, MC, and PU sponge.

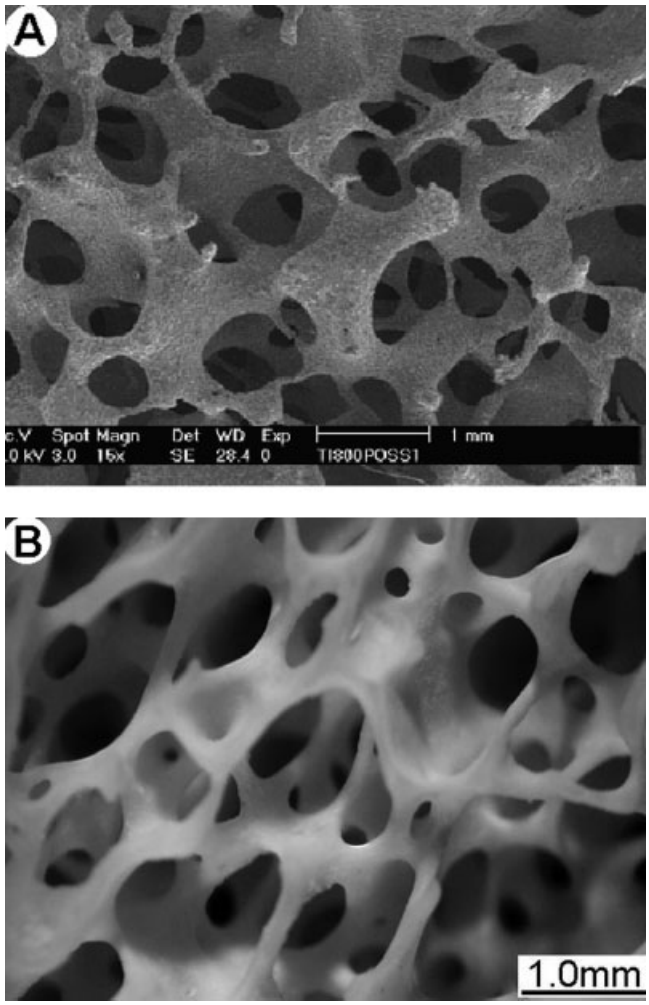

Figure 4. Macrostructure of porous Ti6Al4V and natural bone from goat. (A) Porous Ti6Al4V and (B) cancellous bone from goat.

The porous Ti6Al4V reveals a porous, open-cell structure with a sponge-like appearance. The pores are interconnected. Compared with the macrostructure of cancellous bone [shown in Fig. 4(B)], both structures possess similar interconnected porous structures.

Mean pore size and pore-size distribution indication

An image of a cross-section of the porous Ti6Al4V is shown in Figure 5(A). The mean pore size was measured on surface pores. The distribution indication of pore size is illustrated in Figure 5(B). A majority of pores are between 400 and 700 μm.

Density and porosity

Cylindrical and cubic samples were used, and their weight and volume were measured. The bulk density

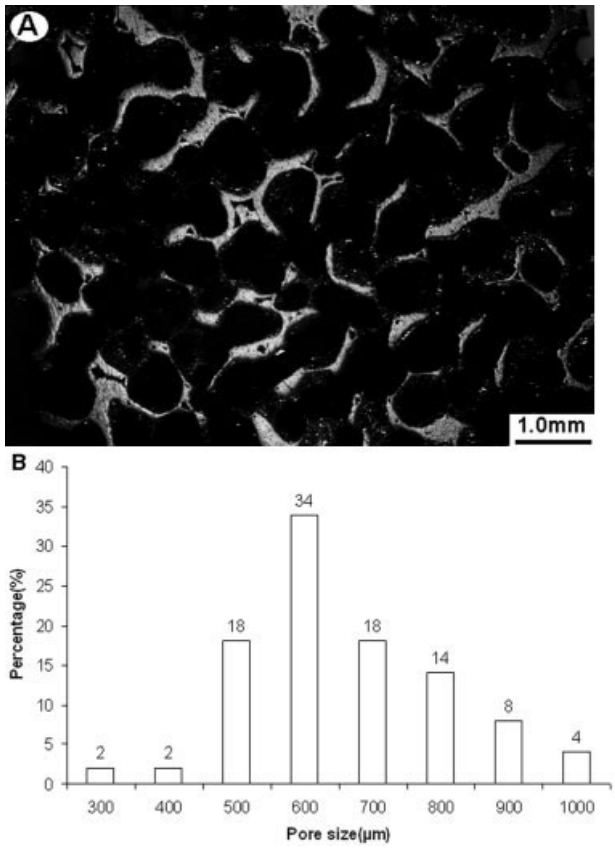

Figure 5. (A) A cross-section of porous Ti6Al4V and (B) pore-size distribution of porous Ti6Al4V.

was 0.49 ± 0.1 g/cm^3. Taking the theoretical density of solid Ti6Al4V as 4.45 g/cm^3, the porosity of porous Ti6Al4V was calculated to be 89 ± 1.6%.

By using image analysis, we estimated the porosity of porous Ti6Al4V to be 91 ± 1.2%. These two methods showed good agreement.

Microstructure of inner surface wall

The microstructure of an inner surface wall is shown in Figure 6. Figure 6(A) indicates that powder bonding is achieved by neck growth through a solid-state diffusion process. No liquid phase occurs. The measured surface roughness (Ra) was 3.4 ± 0.3 μm by equivalent model. Figure 6(B) shows a high magnification of the inner surface of a pore. The voids in the rough surface are referred to as micropores, and their size ranges from 1 to 10 μm.

Elemental analysis

An EDX spectrum was taken from a sample to determine the chemical composition of porous Ti6Al4V after sintering. Figure 6(B) shows the surface (square area) from which the spectrum was acquired and Figure 6(C) shows the spectrum. We can conclude that porous Ti6Al4V after sintering has a typical spectrum of Ti6Al4V. The chemical analysis results of organic residuals (oxygen, hydrogen, carbon, and nitrogen) after the different processing steps are shown in Figure 7. It can be seen that the contents of oxygen, hydrogen, and nitrogen remain nearly unchanged after removal of sponge and binders, and the carbon content increases from 0.02 to 0.08%. After sintering, the concentration of carbon, oxygen, and nitrogen are

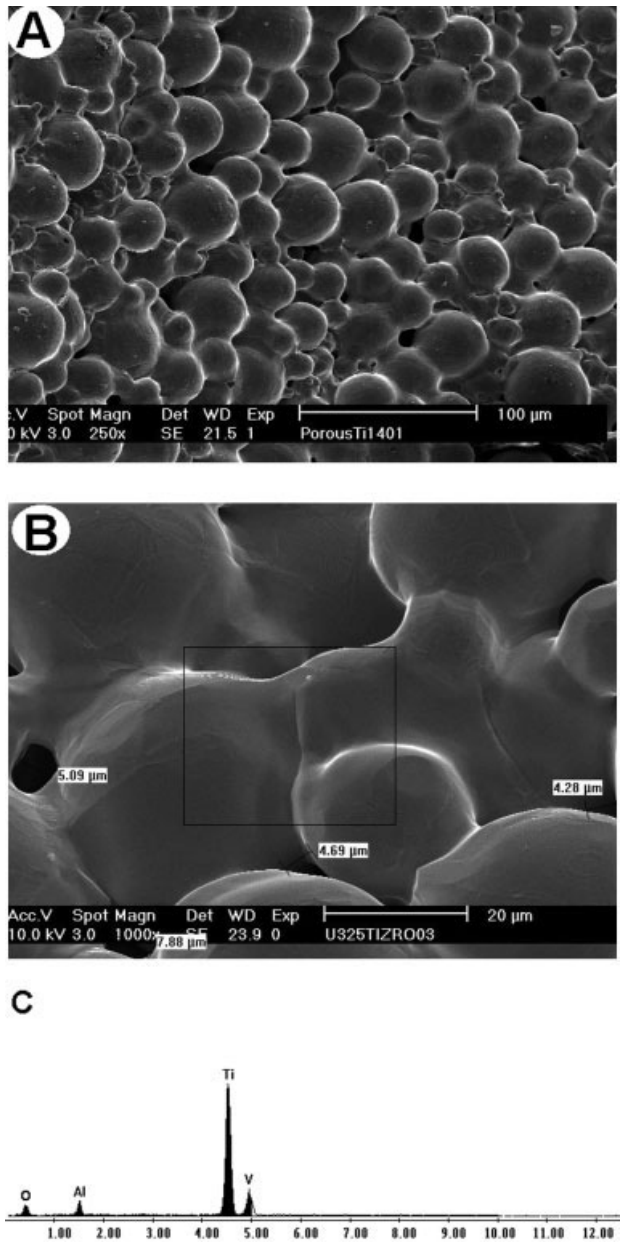

Figure 6. ESEM images of the inner surface of pores and EDX spectrum acquired from the same area. (A) Micropore and rough surface structure, (B) higher magnification (marked area where EDX was taken), and (C) EDX spectrum obtained showing a typical spectrum for Ti6Al4V.

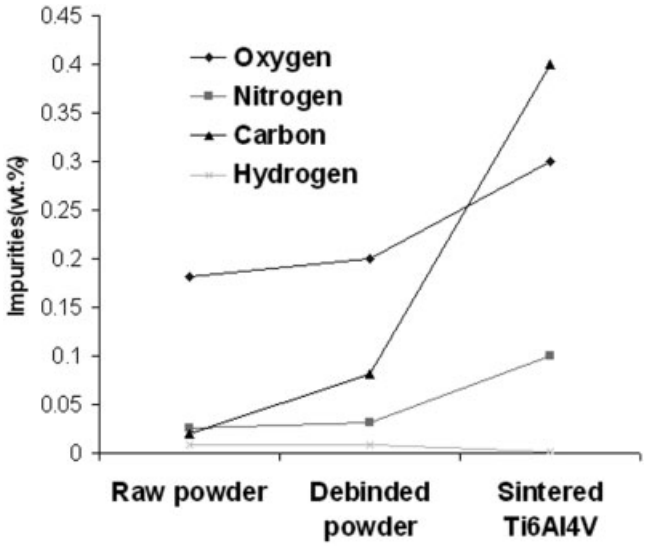

Figure 7. Chemical analysis of oxygen, carbon, hydrogen, and nitrogen contents in Ti6Al4V samples with different steps.

all increased. The reason for this behavior is probably attributable to residual contaminants in the furnace.

Mechanical properties

Figure 8 shows the compressive stress-strain curve of the porous Ti6Al4V with a porosity of 90%. The curve was generally characterized by an initial elastic response, followed by decreasing stress, then a long plateau with a little oscillation where the stress is almost independent of strain, finally a region of densification where the stress-stain curve rises slowly. The average compressive strength of porous Ti6Al4V with a porosity of 90% is 10.3 ± 3.3 MPa. The elastic constant is 0.8 ± 0.3 GPa as calculated from the elastic part of compressive stress-strain curves.

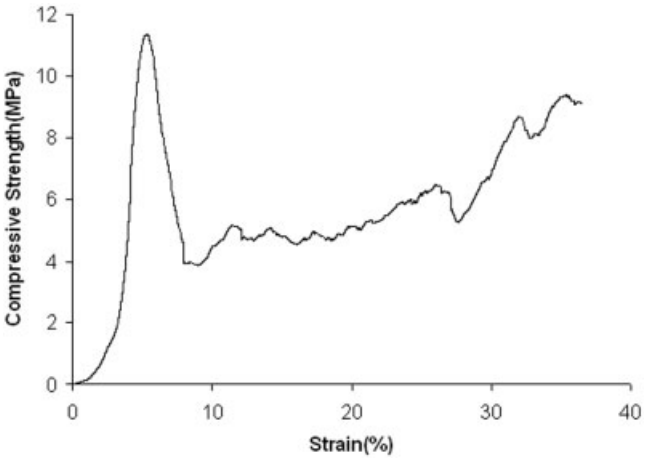

Figure 8. Compressive stress-strain curve of porous Ti6Al4V with a porosity of 90%.

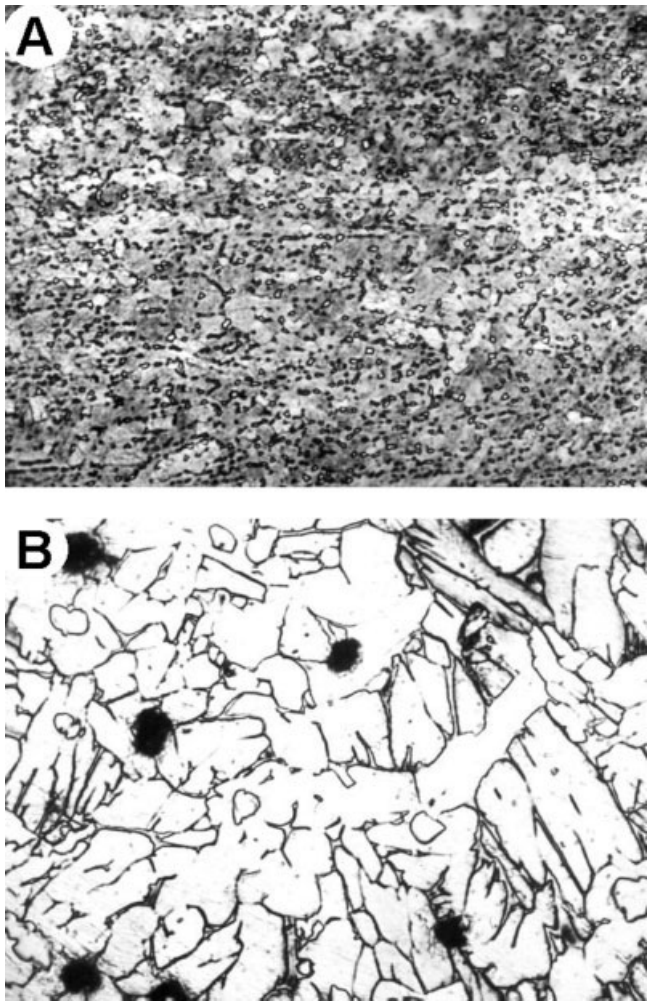

Figure 9. Light micrograph of section: (A) the raw Ti6Al4V without further heat treatment, revealing an equiaxed α-β microstructure and (B) the porous Ti6Al4V revealing a coarse acicular microstructure.

Metallography

The Ti6Al4V plate was found to have an equiaxed α-β microstructure. Figure 9(A) shows the microstructure of a Ti6Al4V plate without any heat treatment. The matrix is α, the small second phase particles are β. The porous Ti6Al4V was found to have a coarse acicular microstructure, revealing α grains with intergranular β phase [shown in Fig. 9(B)].

Cell attachment test

Figure 10 shows ESEM images of cells cultured on the porous Ti6Al4V samples for 4 h [Fig. 10(A)] and 3

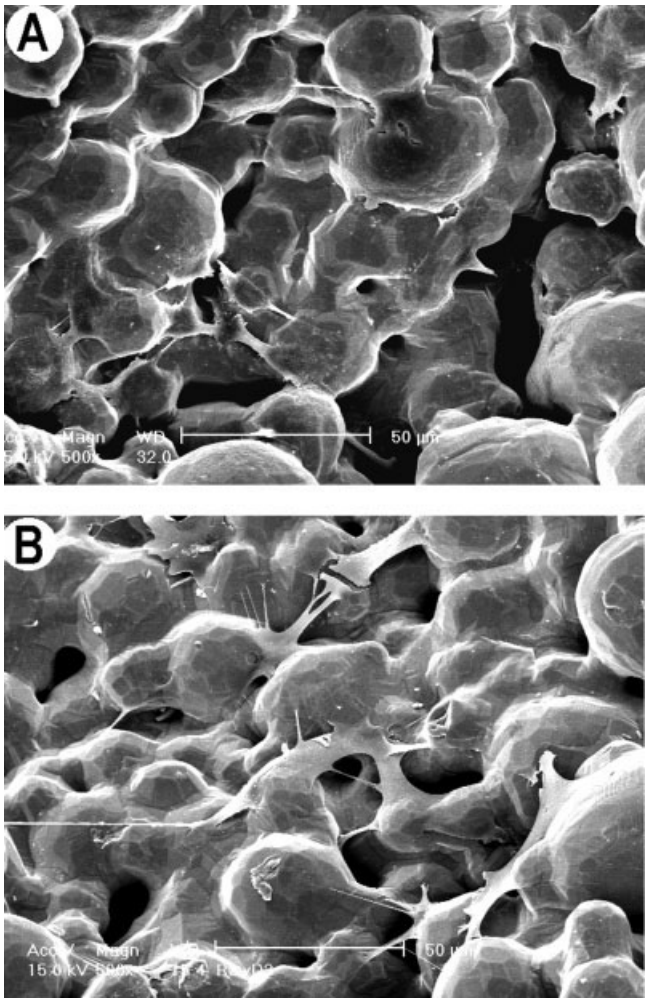

Figure 10. MC3T3-E1 osteoblast-like cells cultured on the porous Ti6Al4V for (A) 4 h and (B) 3 days.

days [Fig. 10(B)]. It can be seen that cells, polygonal and spindle-shaped, attached and spread on the inner surface of porous Ti6Al4V. Meanwhile we can see some cells growing into micropores in the inner surface and the spreading cells maintaining a physical contact with each other by lamellipodia. Cells also formed the extracellular matrix on the surface. No significant difference was found between cells cultured 4 h and 3 days, but DNA content assay (Table III, $R^2 = 0.99$) confirmed that after 3 days of culture more cells were found to attach and spread on the porous Ti6Al4V. Cell attachment test reveals that the cells are not only able to attach and spread well on the inner surface of porous Ti6Al4V, but are also able to form an extracellular matrix.

DISCUSSION

The novel feature of the current technique is that the traditional method of "polymeric sponge replication" producing porous ceramics (porous alumina)[36] was successfully applied for making porous Ti6Al4V. The procedure itself is basically simple: dipping polymeric sponge into Ti6Al4V slurry, then debinding to remove binders and sponge struts, and finally sintering to obtain a porous Ti6Al4V body. The structure resembles the original sponge structure. The porosity is up to 90% with complete open structure.

Normally, at 1250°C, titanium powder bonding is achieved through a solid-state diffusion process. The driving force during this particle-to-particle sintering is a reduction of the local surface energy. When the highly reactive metal reacts with oxygen, carbon, or nitrogen to form brittle surface layers of titanium oxide, carbide, or nitride, this surface energy increases and affects the bonding process as well as ductility and fatigue properties of the final product. To prevent contamination from oxygen, nitrogen, and carbon, we applied a novel method by flushing with high purity of argon gas and titanium hydride particles in the process of debinding and sintering. During the debinding and sintering, titanium hydride was first decomposed to pure titanium and hydrogen starting at 400°C, and almost completed around 600°C. Above 700°C, only little TiH_2 remained to be decomposed.[37–39] The titanium generated by decomposing titanium hydride is more reactive than normal pure titanium or Ti6Al4V, thus reacting with nitrogen, oxygen, and carbon in the chamber before these impurities can react with porous Ti6Al4V. In addition, hydrogen reacted with oxygen.

As a result, the titanium hydride particles act as a scavenger, protecting porous Ti6Al4V from less desirable compounds. Also the flushing high pure argon gas and sintering under a high vacuum has the further advantage of reducing contaminations. Therefore, our enhanced fusion of Ti6Al4V particles may be caused by the absence of titanium carbide and oxides, resulting in increased mechanical properties of the final porous body. It should be noted that the sintering parameters of porous Ti6Al4V alloys can be optimized by further reducing organic residues: this will be the subject of further studies.

Our porous Ti6Al4V created by "polymeric sponge replication" has a three-dimensional reticulate structure with interconnected pores. As stated before, we need both macro- and micropores, because both types of pores also exist in the solid bony skeleton [shown in Fig. 6(A,B)]. Macropores (size and volume) are gener-

TABLE III
DNA Content of Cells Attached on the Porous Ti6Al4V

Culture Time	DNA Content (ng)
4 h	5321.56 ± 295.31
3 days	10678.66 ± 1034.31

ated and controlled by sponge characteristics. By selecting different sponges, we can obtain porous Ti6Al4V with varied pore sizes. Micropores are formed by powder sintering and removal of sponge struts. ESEM shows that the micropore size ranged from 1 to 10 μm. The surface roughness of the pore walls was estimated by measuring the roughness of a model surface consisting of a powder layer sintered onto a flat solid Ti6Al4V plate. The resulting Ra of 3.4 μm gives an indication of the "inner" surface roughness of the pores. Recent studies show that microarchitecture has an important role in the process of bone formation and growth.[40] The microarchitecture of the inner surfaces of pores is favorable for cell seeding, cell attachment, proliferation, differentiation, and ingrowth of tissue.[41]

The porosity of a scaffold influences its mechanical strength according to Gibson and Ashby's model[42] and permeability. Porous Ti6Al4V made by our method has a porosity of 90%, which will be very useful for biomolecules and degraded substances to freely flow into and out of the scaffold. The compressive strength of porous Ti6Al4V in the present study was about 10 MPa, slightly higher than that of cancellous bone.

It is clear that where titanium and its alloy are notch-sensitive materials, the microstructure of these sintered products may well affect mechanical properties such as fatigue strength even more. The necking of the powder particles after sintering and possible residual porosity may present discontinuities where stress concentrations will occur. Also, the sintering process causes the microstructure to transform from a fine equiaxed structure to a lamellar, coarse structure as a result of heating the material above its β phase transition temperature at 992°C with even more detrimental effects on fatigue strength.[43] In loaded application, the fine equiaxed microstructure is certainly preferred in this respect. Several attempts have been made to transform the microstructure to more favorable forms.[44–47] Cook et al.[48] reported that mechanical properties of the porous-coated implant could be improved significantly by the use of postsintering heat treatments directed to reduce α grain size. Still, it must be realized that the use of these porous or porous-coated implants should be confined to applications in which stresses are below the material's fatigue endurance limit and compressive rather than tensile of nature.

All dense metallic alloys used in medical devices have an elastic constant significantly higher than that of bone, although dense Ti6Al4V has a lower elastic constant than other metallic biomaterials used for orthopedic implants.[1–3] The mechanical incompatibility causes implants to be structurally stiffer than bones. The elastic constant of cancellous bone and cortical bone ranges from 0.5 to 30 GPa.[1] The elastic constant of porous Ti6Al4V with a porosity of 90% is between that of cancellous bone and cortical bone. It reveals that porous Ti6Al4V can be made with low elastic constant thereby reducing stress shielding.

Our experimental result of cell attachment showed that the cells attached and spread well on the surface of porous Ti6Al4V. But in *in vitro* experiments, cell attachment tests only give information on cell attachment and the number of cells in the porous Ti6Al4V. Actually, biomaterials implanted in the bone will encounter complicated conditions compared with that *in vitro*, such as more and different cell types, local strain, and pH changes caused by tissue inflammation. Consequently, it is necessary to perform *in vivo* experiments to understand how the bone interacts with our porous Ti6Al4V.

An interesting step in the whole processing route is shaping: the porous Ti6Al4V retained its shape after the supporting sponge was burned out. The reasons can be summarized as follows: 1) powder metallurgy technique was applied for making porous Ti6Al4V. There are some micropores among powders that can overcome collapse during a pyrolysis process, while the polymeric sponge is burning out. There is a space to evaporate gas pyrolyzed by sponge. 2) Binders with two ingredients were used to prepare Ti6Al4V slurry. The two binders were decomposed or evaporated at different temperatures. From TGA curves, it can be seen that first the PEG4000, then the sponge, finally the MC decomposed to avoid collapsing. 3) The rate of heating was precisely controlled to burn out binders and sponge. Because the "green" part is extremely porous, the sintering temperature must be very strictly controlled in order to retain the shape and prevent from "slumping." Removing the binder too fast resulted in blisters, removing it too slowly on the contrary resulted in partial collapsing.[49,50]

CONCLUSIONS

Porous Ti6Al4V was successfully made by integrating a powder metallurgy processing with "polymeric sponge replication." The novel feature of this method lies in the fact that the structure of porous Ti6Al4V body can be directly replicated from that of sponge structure. The porous Ti6Al4V made in such a way possesses a completely open pore, high porosity (~90%), reticulate porous structure. This structure is similar to that of cancellous bone. The compressive strength is 10.3 ± 3.3 MPa, and the elastic constant is between that of cancellous bone and cortical bone. *In vitro*, experiments show that the porous Ti6Al4V is not only nontoxic but also favorable for cell attachment. The porous Ti6Al4V fabricated by this method is ex-

pected to be a very promising biomaterial for orthopedic implants.

The authors thank IsoTis S.A. for the financial support. The authors also thank Fabienne Peters for her enthusiastic help in the TGA experiments and Dr. Jiawei Wang for cell attachment experiments. The discussions with Dr. Huipin Yuan were also very constructive during the preparation of this article.

Reference

1. Long M, Rack HJ. Titanium alloys in total joint replacement: a materials science perspective. Biomaterials 1998;19:1621–1639.
2. Gu H, Xu G. Biomedical material science. Tianjin: Science Translation Press; 1993.
3. Wilke A, Landgraff M, Orth J, Kienapfel H, Grissand P, Franke R. Human bone marrow cell cultures: a sensitive method for determination of the biocompatibility of implant materials. ATLA 1999;27:137–151.
4. Pilliar RM. Powder metal-made orthopedic implants with porous surface for fixation by tissue ingrowth. Clin Orthop 1983; 176:42–51.
5. Pilliar RM, Cameron HU, Welsh RP, Binnington AG. Radiographic and morphologic studies of load-bearing porous-surfaced structured implants. Clin Orthop 1981;156:249–257.
6. Murray GA, Semple JC. Transfer of tensile loads from a prosthesis to bone using porous titanium. J Bone Joint Surg Br 1981;63-B(1):138–141.
7. Maniatopoulos C, Pilliar RM, Smith DC. Threaded versus porous-surfaced designs for implant stabilization in bone-endodontic implant model. J Biomed Mater Res 1986;20(9):1309–1333.
8. Maniatopoulos C, Pilliar RM, Smith DC. Evaluation of shear strength at the cement-endodontic post interface. J Prosthet Dent 1988;59(6):662–669.
9. Maniatopoulos C, Pilliar RM, Smith DC. Evaluation of the retention of endodontic implants. J Prosthet Dent 1988;59(4): 438–446.
10. Pilliar RM, Cameron HU, Macnab I. Porous surface layered prosthetic devices. Biomed Eng 1975;10(4):126–131.
11. Simmons CA, Valiquette N, Pilliar RM. Osseointegration of sintered porous-surfaced and plasma spray-coated implants: an animal model study of early postimplantation healing response and mechanical stability. J Biomed Mater Res 1999; 47(2):127–138.
12. Clemow AJ, Weinstein AM, Klawitter JJ, Koeneman J, Anderson J. Interface mechanics of porous titanium implants. J Biomed Mater Res 1981;15(1):73–82.
13. Bobyn JD, Pilliar RM, Cameron HU, Weatherly GC, Kent GM. The effect of porous surface configuration on the tensile strength of fixation of implants by bone ingrowth. Clin Orthop 1980(149):291–298.
14. Katz JL, Pilliar RM, Berkowitch J, Christel P, Higham P, Kempeneers R, Knox GF, Scott I, Sudanese A. Biomechanical stability and design. Stiffness and remodelling. Ann NY Acad Sci 1988;523:283–286.
15. Cameron HU, Pilliar RM, Macnab I. The rate of bone ingrowth into porous metal. J Biomed Mater Res 1976;10(2):295–302.
16. Chen PQ, Turner TM, Ronnigen H, Galante J, Urban R, Rostoker W. A canine cementless total hip prosthesis model. Clin Orthop 1983(176):24–33.
17. Landon GC, Galante JO, Maley MM. Noncemented total knee arthroplasty. Clin Orthop 1986(205):49–57.
18. Bobyn JD, Cameron HU, Abdulla D, Pilliar RM, Weatherly GC. Biologic fixation and bone modelling with an unconstrained canine total knee prosthesis. Clin Orthop 1982(166):301–312.
19. Hahn H, Palich W. Preliminary evaluation of porous metal surfaced titanium for orthopedic implants. J Biomed Mater Res 1970;4(4):571–577.
20. Galante J, Rostoker W, Lueck R. Sintered fiber metal composites as a basis for attachment of implants to bone. J Bone Joint Surg Am 1971;53(1):101–114.
21. Welsh RP, Pilliar RM, Macnab I. Surgical implants. The role of surface porosity in fixation to bone and acrylic. J Bone Joint Surg Am 1971;53(5):963–977.
22. Wu BD, Cui YF. Research on porous titanium for medical implant material. Rare Met Mater Eng 1988;4:55–58.
23. Wu BD, Guo FH. A study of preparation of man-made hipbone by using composite porous titanium. Technol Powder Metall 1990;8(4):145–149.
24. Pilliar RM. Overview of surface variability of metallic endosseous dental implants: textured and porous surface-structured designs. Implant Dent 1998;7(4):305–314.
25. Pilliar RM, Deporter DA, Watson PA, Todescan R. The Endopore implant-enhanced osseointegration with a sintered porous-surfaced design. Oral Health 1998;88(7):61–64.
26. Pilliar RM. P/M processing of surgical implants: sintered porous surfaces for tissue-to-implant fixation. Int J Powder Metall 1998;34(8):33–45.
27. Asaoka K, Kuwayama N, Okuno O, Miura I. Mechanical properties and biomechanical compatibility of porous titanium for dental implants. J Biomed Mater Res 1985;19(6):699–713.
28. Oliveira MV, Pereira LC, Cairo CAA. Porous structure characterization in titanium coating for surgical implants. Mater Res 2002;5(3):269–273.
29. Oh IH, Nomura N, Masahashi N. Mechanical properties of porous titanium compacts prepared by powder sintering. Scr Mater 2003;49:1197–1202.
30. Ducheyne P, Willems G, Martens M, Helsen J. *In vivo* metal-ion release from porous titanium-fiber material. J Biomed Mater Res 1984;18(3):293–308.
31. Kuo KN, Gitelis S, Sim FH. Segmental replacement of long bones using titanium fiber metal composite following tumor resection. Clin Orthop 1983;176:108–114.
32. Galante J, Rostoker W. Fiber metal composites in the fixation of skeletal prosthesis. J Biomed Mater Res 1973;4:43–61.
33. Matin B, Cornelia S, Bronkremer HP, Baur H. High-porosity titanium, stainless steel, and superalloy parts. Adv Eng Mater 2000;2(4):196–199.
34. Engh CA. Hip arthroplasty with a Moore prosthesis with porous coating. Clin Orthop 1983;176:52–66.
35. Pilliar RM. Porous-surfaced metallic implants for orthopedic applications. J Biomed Mater Res 1987;21(A1 Suppl):1–33.
36. Kwon S-H, Jun Y-K, Hong S-H. Calcium phosphate bioceramics with various porosities and dissolution rates. J Am Ceram Soc 2002;85(12):3129–3131.
37. Akiyama S, Imagawa K, Kitahara A, Nagata S. Morimoto SK, Nishikawa T, Itoh M. Foamed metal and method of producing the same. US Patent 4,713,277. 1987.
38. Gergely V, Curran DC, Clyne TW. The FOAMCARP process: foaming of aluminium MMCS by the chalk-aluminium reaction in precursors. Comp Sci Technol 2003;63(16):2301–2310.
39. Mu W, Deng GZ, Luo FC. Titanium metallurgy. Beijing: Metallurgy Industry Press; 1998.
40. Wilson CE, De Bruijn JD, Kruijt M, Van Blitterswijk CA, Verbout AJ, Dhert WV. Design and fabrication of standardized hydroxyapatite scaffolds with a defined macro-architecture by rapid prototyping for bone-tissue-engineering research. J Biomed Mater Res 2004;68A:123–132.
41. Zhang C, Wang J, Zhang X. Osteoinductivity and biomechanics of a porous ceramic with autogenic periosteum. J Biomed Mater Res 2000;52:354–359.

42. Gibson LJ, Ashby MF. Cellular solids: structure and properties. Cambridge: Cambridge University Press; 1997.
43. Weinstein AM, Klawitter JJ, Koeneman JB. Structure properties relationship for porous Ti6Al4V. In: Proceedings of the Third Annual Meeting of the Society for Biomaterials; 1977; New Orleans, LA.
44. Cook SD, Anderson RC, Thongpreda N, Haddad RJ Jr. The effect of post-sintering heat treatments on the tensile properties of Ti-6A1-4V alloy. Biomater Med Devices Artif Organs 1986; 14(3–4):167–180.
45. Cook SD, Renz EA, Haddad RJ. Post-sintering heat treatments for porous coated Ti-6A1-4V alloy. Biomater Med Devices Artif Organs 1985;13(1–2):37–50.
46. Kohn DH, Ducheyne P. A parametric study of the factors affecting the fatigue strength of porous coated Ti-6A1-4V implant alloy. J Biomed Mater Res 1990;24(11):1483–1501.
47. Kohn DH, Ducheyne P. Materials for bone and joint replacement. In: Williams DF, editor. Materials science and technology. A comprehensive treatment. New York: VCH Publications; 1992. p 31.
48. Cook SD, Thongpreda N, Anderson RC, Haddad RJ Jr. The effect of post-sintering heat treatments on the fatigue properties of porous coated Ti-6Al-4V alloy. J Biomed Mater Res 1988;22(4):287–302.
49. Lin JY, Zhang Y. Effect of fabrication technology on the structures and properties of TiC ceramics foam. Powder Metall Technol 2000;18(1):12–15.
50. Wegmann G, Gerling R, Ebel T, Karl-Heinz O. Metal injection moulding of titanium alloys for medical applications. In: Proceedings from Europe Advance Materials Week Conference; 2001; Munich, Germany.